

Full length article

Cyclic test and numerical analytical assessment of cold-formed thin-walled steel shear walls using tube truss

Jingfeng Wang^{a,b,*}, Wanqian Wang^a, Yaming Xiao^{a,c}, Bo Yu^a^a School of Civil Engineering, Hefei University of Technology, Anhui Province 230009, China^b Anhui Civil Engineering Structures and Materials Laboratory, Anhui Province 230009, China^c Anhui Collaborative Innovation Center Advanced Steel Structure Technology and Industrialization, Anhui Province 230009, China

ARTICLE INFO

Keywords:

Cold-formed thin-walled steel tube truss (CFSTT)
Shear wall
Cyclic behavior
Finite element (FE) modeling
Parametric studies

ABSTRACT

Cold-formed thin-walled steel tube truss (CFSTT) shear walls are gradually used in some engineering practice (i.e. residence, supermarket, school etc.) owing to their superiorities such as light weight, better ductility and easy construction. However, little attention to the seismic behavior and parametric influence of the CFSTT shear walls has been paid. In this paper, a series of cyclic tests and numerical analysis were conducted to investigate structural performance of the CFSTT shear walls. Five full-scale CFSTT shear walls sheathed with double-side oriented strand board (OSB) panels and one pure CFSTT skeleton wall were tested under constant axial compression combining lateral cyclic load. Failure pattern, horizontal load versus displacement relationship and ductility of the test specimens were analyzed and assessed. The experimental data showed that the CFSTT shear walls behaved good hysteretic behavior, ductility and energy dissipation. Following this, a nonlinear finite element (FE) analysis modeling of the type of cold-formed shear wall was developed, and the accuracy of the FE models was verified by experimental data. Parametric studies were conducted to explore the effect of X-shaped bracing number, OSB panel thickness, sheathing type, etc. on the shear bearing capacities and elastic stiffness of the CFSTT shear walls. The results indicated that the shear bearing capacity and elastic stiffness of the CFSTT shear wall were obviously affected by number of X-shaped bracing, four-limb lattice stud, thickness of OSB panel and the type of sheathing. The experimental and analytical results may promote the design and application for CFSTT shear walls in engineering practice.

1. Introduction

In recent years, the development of building industrialization has promoted the innovation of prefabricated wall panels in China and other countries. The cold-formed thin-walled steel (CFS) shear wall, as one of the main products using C-shaped steel wall stud, was popularly used in the low-rise buildings accounting for excellent structural advantages, such as high strength, light weight, fairly high standardization, efficient energy saving and superior earthquake-resistance [1]. However, it is well known that the C-shaped steel exhibits poor torsional performance under bending and compressive loads. Moreover, initial imperfection of C-shaped steel behaves significant influence on the performance of CFS shear walls. Consequently, novel cold-formed thin-walled steel tube truss (CFSTT) shear wall was invented and applied to enhance the shear wall resistance by changing C-shaped steel into square steel tube.

The CFSTT shear wall was a light-gauge wall with certain spacing of

double or four limb lattice studs, which was introduced into China from Canada for its applicability in some residences and supermarkets. The CFSTT structures were designated by Carter charity fund as its specified product [2,3]. The CFSTT shear wall (illustrated in Fig. 1) consists of double-side OSB panels, wall studs, top and bottom tracks. Besides, the wall stud is composed of double or four square tubes and galvanized V-shaped connectors. The double OSB panels were connected with the CFSTT skeleton members by self-drilling screw. The type of cold-formed steel shear wall behaves all advantages of conventional CFS shear walls and moreover shows better architectural aesthetics appearance, good economical efficiency as well as superior structural stability. Therefore, some engineers and architects radiated an increasingly favor to use the CFSTT shear walls in low-rise and multi-storey buildings.

Up to now, previously published literatures related with the CFS structures were mainly focused on the shear walls adopting C-shaped cold-formed steel as the wall stud. A series experiments had been carried out on the CFS shear walls under diverse load conditions. The static

* Corresponding author at: School of Civil Engineering, Hefei University of Technology, Anhui Province 230009, China.
E-mail address: jfwang008@163.com (J. Wang).

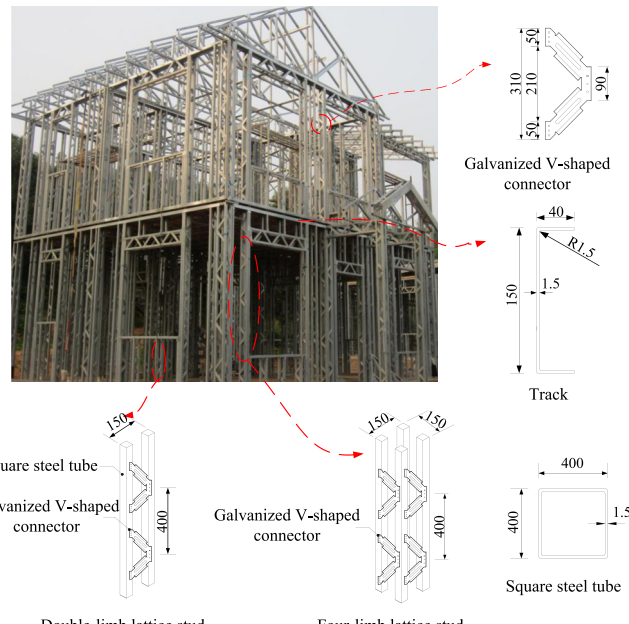


Fig. 1. Main members of CFSTT frame.

behavior of the CFS-framed shear walls sheathed with different type of panels was respectively explored by Lee and Miller [4] and Tian et al. [5,6]. Besides, a plenty of studies on the hysteretic performance of the CFS shear walls were conducted to explore their failure modes and cyclic performance, such as Wang and Ye [7], Nithyadharan and Kalyanaraman [8], Macillo et al. [9]. In Ref. [9], four full-scale CFS shear walls sheathed with gypsum-based panels were tested, and the influence of the aspect ratio, the type of loading and the effect of finishing was investigated. The shake table tests were also conducted on cold-formed steel framed buildings by researchers such as Schafer et. al [10] and Kim et. al [11]. Apart from these above-mentioned work, extensive investigations have been carried out on kinds of alternatives to the CFS shear walls, including steel skeleton [12], sheathing type [13], infill material [14], opening [15], connections [16–20], strap-braced [21] and construction measure [22,23]. However, few literatures on the experimental response of the CFSTT shear walls have been reported. Hence, the investigation on the type of shear walls is of inevitable necessity. On the other hand, owing to complex process and larger expense of experimental models and apparatus, numerical analysis would be an extremely powerful and effective way for in-depth study to better understand the performance of CFSTT shear walls, which was used preferentially for analyzing the behavior of the CFS shear walls [24,25]. Therefore, to explore the properties of the CFSTT shear walls efficiently, a demand for establishing a finite element (FE) modeling on the type of shear wall is emerged as well.

The main object of this paper is to make a further investigation on the seismic performance of CFSTT shear walls. Hereinto, five full-scale CFSTT shear wall specimens with double-side OSB sheathings and one CFSTT skeleton wall specimen were tested under vertical axial compression combining lateral cyclic load. The seismic behavior of CFSTT shear walls was estimated in terms of failure mode, hysteretic curve, ductility and energy dissipation. A FE analysis modeling for analyzing the performance of the CFSTT shear wall was developed, and the accuracy of the FE models was verified by the test results in the field of failure modes and load displacement relationship curves. In addition, extensive parametric analysis was utilized to explore the effect of various parameters on the shear wall, such as X-shaped bracing number, OSB panel thickness and sheathing type. The analysis results may be of

great importance for improving the design level of CFSTT shear walls and provide a useful reference for engineering practice.

2. Experiment description

2.1. Test specimens

According to practical engineering, five single-storey full-scale CFSTT shear walls with double-side OSB sheathings and one pure CFSTT skeleton wall were tested and analyzed in this section to explore seismic performance and failure pattern of the type of shear walls. All specimens were tested under axial compression combining lateral cyclic load. The detail information of test specimens was illustrated in Fig. 2. All the test specimens were 4.2 m wide and 3.25 m high. Table 1 listed specimen information, including the opening size, opening area ratio and sheathing type.

The wall studs were composed of two or four cold-formed thin-walled square steel tubes $\square 40 \times 40 \times 1.5$ mm connected by galvanized V-shaped connectors (1.5 mm thick). Besides, double-limb lattice studs were used at the interior locations placed at 0.61 m on center; while four-limb lattice studs were used at the wall and opening boundaries according to specification DB34/T 647–2006 [26]. All frame members consisted of cold-formed steel profile. According to the specification GB/T 15856–2002 [27], the frame members were connected by ST4.2-grade ($d=4.2$ mm) self-drilling screws. Top and bottom tracks were made by identical U-section of dimension $150 \times 40 \times 1.5$ mm. The X-shaped bracing on both sides of the wall frame were 100 mm wide and 1.5 mm thick. 1.5 mm thick gusset plates were used to strengthen the connection with the aid of X-shaped bracings. Specimens CFSTT1–CFSTT5 were sheathed with 8 mm thick OSB panels. The OSB panels were attached with ST4.2 self-drilling screws spaced at 150 mm along the perimeter and spaced at 300 mm in the field of the panels. To accommodate openings, the panels were cut to fit up and down the doors and windows.

The shear capacity of steel-to-steel connection was calculated by Eq. (1) according to the specification GB50018 [28], and the shear capacity of steel-to-sheathing connection was calculated by Eq. (2) in accordance with Shi [29]. The shear capacity of steel-to-steel connection and steel-to-sheathing connection were 4.37 kN and 0.39 kN, respectively.

$$N_v^f = 3.7(t_1^3 d)^{1/2} f_1 \quad (1)$$

$$P = t_2 d f_2 \quad (2)$$

where: N_v^f is shear capacity for single screw connections; t_1 is the thickness of steel; d is the diameter of the self-drilling screw; f_1 is tensile strength of steel; P is shear capacity for single screw connections of steel-to-sheathing; t_2 is the thickness of sheathing; f_2 is static bending strength of sheathing.

2.2. Material properties

The steel material properties of the CFSTT components were tested based on the specification GB/T228.1–2010 [30]. Three tensile coupons were cut from the specimen for uniaxial tensile test, the purpose of uniaxial tensile test was to determine the yield stress (f_y), the ultimate stress (f_u), elastic modulus (E), and the elongation at fracture (δ). It should be noted that steel materials in the type of shear wall mainly included the steel skeleton, the steel strip and V-shaped connector. The data of the material tests were listed in Table 2. The stresses (σ) and strains (ϵ) curves were obtained from the coupon tests as depicted in Fig. 3.

The material properties of the OSB panel were obtained: yield strength was 7.86 N/mm²; elastic modulus was 3500 N/mm²; Poisson's ratio was 0.3; and density was 650–740 kg/m³.

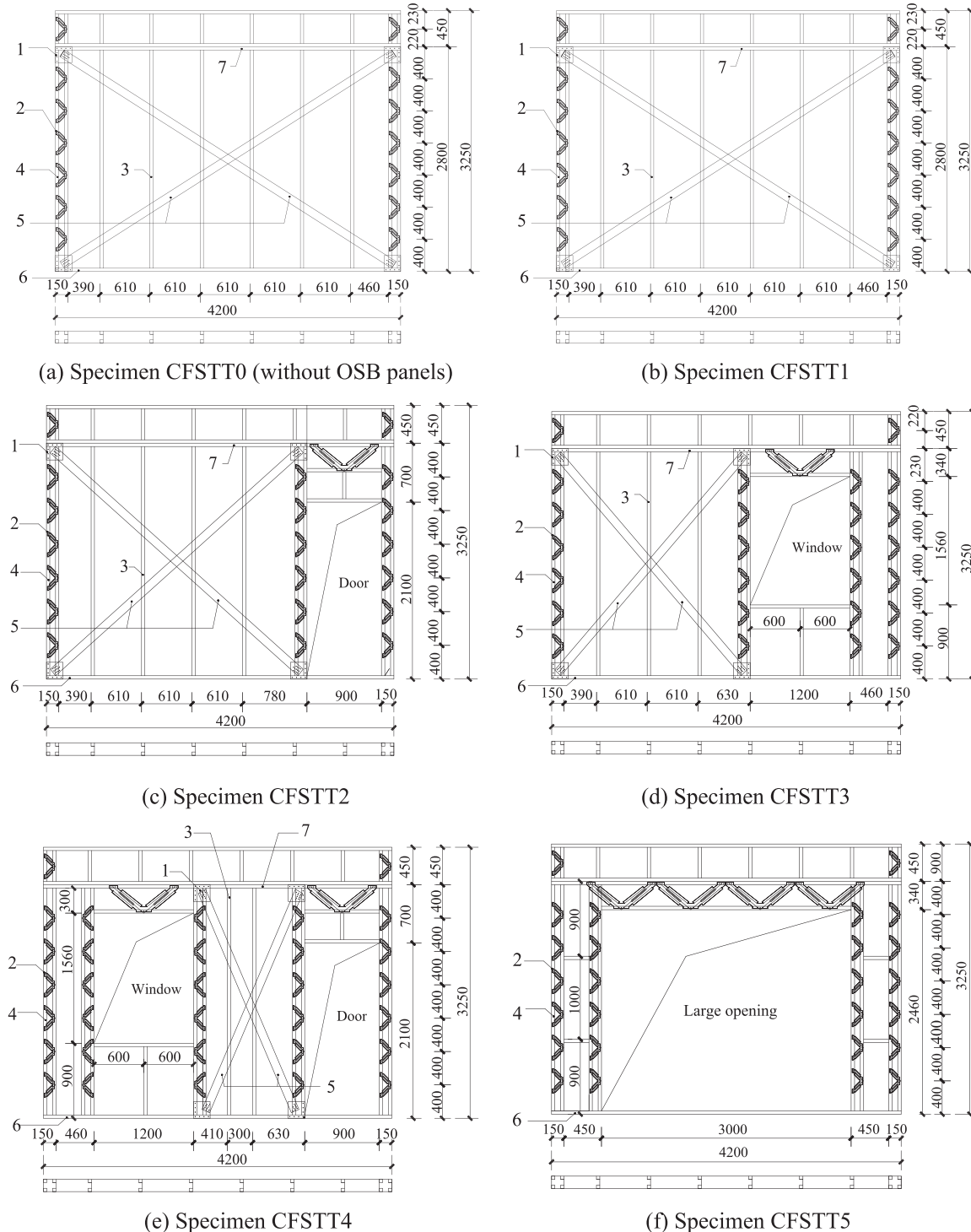


Fig. 2. Details of wall specimens (units: mm). Note: 1-Gusset plate, 2-Galvanized V-shaped connector, 3-Double-limb lattice stud, 4-Four-limb lattice stud, 5-X-shaped bracing, 6-Bottom track, 7-Top track.

2.3. Test setup and loading procedure

The experiments were performed in Anhui Civil Engineering Structures and Materials Laboratory. The test setup was shown in Fig. 4. One 1000 kN MTS hydraulic actuator with a displacement range of ± 250 mm was mounted on the reaction wall to exert the lateral cyclic load to the wall. All tests loading were controlled by displacement. Four 32 mm diameter steel bars were used to transfer load between hydraulic actuator and specimen. The tracks of the test specimens were connected to the bottom foundation beam by eight Grade 8.8 M16 bolts to

facilitate the transfer of horizontal shear load, and the displacement of the shear wall bottom is restricted by the tension anchors and bottom foundation beam. A 500 kN hydraulic jack was suspended off the reaction beam and was placed on the distributive girder to impose axial load on the wall. The distributive girder was 2.4 m length and was identified by box-section of dimension $300 \times 250 \times 10 \times 10$ mm.

The axial pressure of 170 kN (except for the weight of distributive girder), which was calculated from the typical structural according to the actual project, was gradually applied to the top of the shear wall. The dead loads contain the dead weight of floor, columns, beams and

Table 1
Description of test specimens.

Specimen label	Opening size (mm × mm)		Opening area ratio	Panel type	Sheathing type
	Door	Window			
CFSTT0	—	—	—	—	—
CFSTT1	—	—	—	OSB	Double side
CFSTT2	900 × 2100	—	13.8%	OSB	Double side
CFSTT3	—	1200 × 1560	13.9%	OSB	Double side
CFSTT4	900 × 2100	1200 × 1560	27.8%	OSB	Double side
CFSTT5	3000 × 2420	—	54.6%	OSB	Double side

shear walls of the structure, while the live loads consist of snow load and live load of floor. In the loading phase, triangular waves were used for displacement control according to loading history, which was generally applied in accordance with the ATC-24(1992) [31] guidelines for cyclic testing of structural steel components (shown in Fig. 5). Δ_y was defined as the predicted yielding displacement corresponding to the predicted yielding load (P_y), and P_y was approximately $0.7P_{max}$ (P_{max} denotes the predicted ultimate loading capacity on the basis of finite element analysis).

Four linear variable differential transformers (LVDT) were used to measure the displacement of the specimens during the test. The layout of the LVDTs is illustrated in Fig. 4(b). LVDT #1 (D1) measured the horizontal displacement of the top of the wall. LVDT #2 (D2) measured the horizontal displacement of the bottom track of the specimen. LVDT #3 and #4 (D3 and D4) was used to measure the side-sway of the wall.

3. Analysis of experimental results

3.1. Failure pattern

Failure patterns of CFSTT shear walls (seen in Fig. 6) were investigated based on the test phenomena in this section. The test result showed that the sheathing panels of all walls exhibited bulging at low load levels. For specimen CFSTT1 without openings named that CFSTT skeleton sheathed with double-side 8 mm thickness OSB panels, slight screws pull-through and detachment of panel from frame was observed with the lateral displacement increasing. When unloading to the zero, the OSB panels recovered to the original stage. In accompanied with screws pull-through and detachment of panel from frame, separating of sheathing appeared resulting in a descent of shear bearing capacities. Then a sharp noise owing to extrusion between the OSB panels was sent out with an increase of the lateral displacement. After further increase of lateral displacement, vertical cracks and tearing on the OSB panels were observed owing to mutual extrusion. By the end of the test, screw pulled out and the OSB panel appeared serious shedding and detached from frame. The wavy-shape and fracture among the double-limb lattice studs of X-shaped bracing were observed. Furthermore, the buckling of top and bottom track appeared near the four-limb lattice studs. Detail failure patterns of specimen CFSTT1 were depicted in Fig. 6(b).

In term of the specimen CFSTT0, the steel strip appeared yield firstly. As the test continued, the four steel strips on both sides of the wall showed different degrees of relaxation, and behaved in wave shapes. The test of specimen CFSTT0 was terminated with signs that severe local buckling appeared on the four-lime lattice stud and the bottom track appeared local buckling (seen in Fig. 5a).

For the CFSTT shear wall with openings, screw pull-through and detachment of panel from frame in specimens CFSTT2, CFSTT3 and CFSTT4 was earlier than that of specimen CFSTT1. The crack of the OSB panels in specimens with various types of openings was first observed around the openings margin angles where lager tension field forces existed. It should be stressed that the buckling appeared at lower load levels contrast to specimen CFSTT1 owing to the stress concentration around sharp opening corners. For specimen with openings, serious bending of angle steel at the corner of the opening was observed; two self-drilling screws on angle steels were pulled out adjacent to the four-limb lattice stud, as shown in Fig. 6(d). With regard to specimen CFSTT5, slight tearing in OSB panels was observed within the vicinity of opening when the displacement arrived at 35 mm. Eventually, the obvious screw pull-through, detachment of panel from frame, and bulking of the tracks around the four-limb lattice stud were also observed.

3.2. Load-displacement hysteretic curve

The force-displacement hysteresis relationship can reflect the cyclic performance of the CFSTT shear walls obviously, as shown in Fig. 7. The drifts were defined as drift = Δ/h . In which, Δ is the measured displacement in the top of the wall; h is the calculated height of the wall. The shapes of the curves were stable and plentiful with a noticeable pinching effect. It could be seen that strength degradation may be attributed to cracks of OSB panel, screws pull-through and detachment of panel from frame, fracture of steel strips, and buckling of top and bottom tracks. Specimen CFSTT1 had a plumper hysteresis loops compared with other specimens. The pinching effect on the hysteresis loops for specimen CFSTT0 was more obvious, and this may be attributed to the absence of OSB panels. Furthermore, the hysteretic curves of specimens CFSTT2, CFSTT3 and CFSTT4 were similar to each other, and the major contribution to this result may come from the setting of four-limb lattice stud. Moreover, the specimen CFSTT5 appeared an apparent degradation of shear capacity and lateral stiffness with respect to specimen CFSTT1, which indicated that the hysteretic behavior might be obviously influenced by large opening. Consequently, it can be concluded that the hysteretic curves were related to the opening rate and the number of four-limb lattice stud.

3.3. Load-displacement envelop curve and ductility

The horizontal load-displacement envelope curves (seen in Fig. 8) of test specimens were obtained by connecting peak load point at each displacement level according to the load-displacement hysteretic curves

Table 2
Material properties of steel.

Steel components	Steel wall thickness (mm)	Yield strength f_y (N/mm ²)	Ultimate stress f_u (N/mm ²)	Elastic modulus E (N/mm ²)	Elongation at fracture δ (%)
Steel strip	1.5	216	314	1.85×10^5	32
Steel skeleton	1.5	300	330	2.02×10^5	19
V-shaped connectors	1.5	361	374	2.45×10^5	19

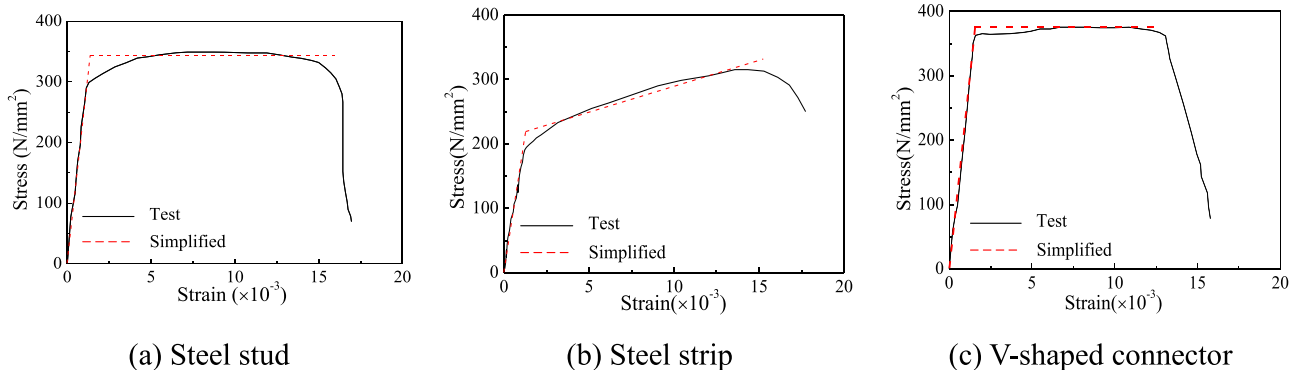


Fig. 3. Stress-strain curves of shear wall components.



(a) Overview of test specimen

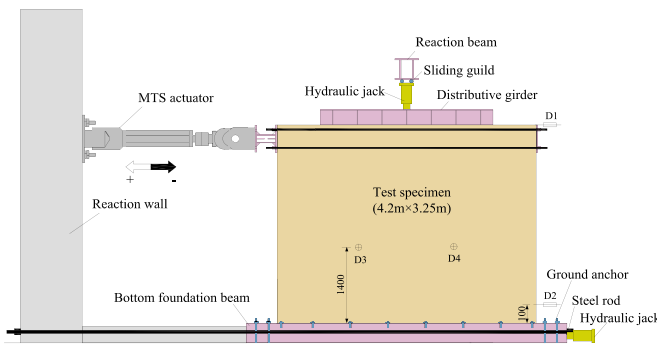


Fig. 4. Experimental setup. Note: '(+)' and '(-)' mean 'Positive Direction' and 'Negative Direction', respectively.

(shown in Fig. 7). In order to determine feature points from the envelope curves to evaluate earthquake resistance of the specimens quantitatively, three typical characteristic points (yield point, peak point and failure point) were introduced according to specification JGJ/T 101 [32] (shown in Fig. 9). Three typical characteristic points of each specimen in accordance with envelop curves are summarized in Table 4. According to the test results, specimen CFSTT1 shows greater shear bearing capacity and elastic stiffness than other specimens. The comparison between envelope curves of specimen CFSTT1 and CFSTT0 demonstrated that OSB panels had significant contribution to the wall stiffness. Specimen CFSTT5 exhibits the lowest shear bearing capacity and elastic stiffness due to largest opening ratio. It indicates that the wall opening decreases the shear bearing capacity and elastic stiffness of CFSTT shear wall significantly. Besides, the shear bearing capacity and elastic stiffness are related to the opening type and the amount of four-limb lattice stud. When the opening area is small, the seismic

performance can be significantly improved by setting four-limb lattice studs at both sides of the opening instead of double-limb lattice studs. When the opening area is large, setting up four-limb lattice studs has slight influence for improving its seismic performance. Moreover, the large opening has more obvious detrimental influence on the elastic stiffness and shear bearing capacity of CFSTT shear wall. It is recommended that the suitable measures are needed to be taken to improve the seismic behavior of CFSTT shear wall with openings.

The displacement ductility factor (μ) was adopted to evaluate the ductility property of the type of shear wall. The ductility of CFSTT shear wall was evaluated by the ductility factor (listed in Table 2), namely $\mu = \Delta_{f,t}/\Delta_{y,t}$. Table 2 shows that specimen CFSTT1 has higher ductility than specimen CFSTT0 because of the stressed skin diaphragm. Whilst, the ductility of specimens CFSTT2, CFSTT3, CFSTT4 and CFSTT5 are visibly raised, compared to specimen CFSTT1. The evidence indicates that openings and four-limb lattice stud have beneficial effect on the ductility of CFSTT shear wall. The test data exhibits that the displacement ductility factor (μ) of all test specimens is in the scope of 3.22–9.15. Up till now, there were none of detail ductility regulations for the CFSTT shear wall. Thus, compared the results in this paper with the Li and Yang [15], it indicates that the type of shear walls exhibit a good deformability and can satisfy the seismic design requirements of structures.

3.4. Energy dissipation capacity

The equivalent damping coefficient (ξ_e) adopted in specification JGJ101 [33] was calculated by Eq.(3). The idealized load-deflection relationship may be described as shown in Fig. 10. Table 3 shows the total dissipation energy W_{total} , the equivalent damping factor (ξ_e) and the energy-dissipating capacity (E_e) of all specimens.

$$\xi_e = \frac{1}{2\pi} \frac{S_{ABC} + S_{CDA}}{S_{OBE} + S_{ODF}} \quad (3)$$

$$E_e = 2\pi\xi_e \quad (4)$$

The total dissipated energy W_{total} of the specimens estimated by the areas of the horizontal load versus displacement hysteretic loops and W_{total} is defined as the areas of the hysteresis curves at failure state. Based on the total dissipation energy W_{total} (listed in Fig. 11), observation can be drawn as follows: The dissipated energy capacity of specimen CFSTT1 is apparently higher than that of specimen CFSTT0, which indicates that the skin diaphragm has significant influence on energy dissipation. It can be seen that the dissipation energy W_{total} of specimens CFSTT3 and CFSTT4 is higher compared to specimen CFSTT5, while the dissipation energy W_{total} of the specimen CFSTT2 is lower than CFSTT5. The result showed that large opening has an extremely negative impact on energy dissipation of the CFSTT shear wall, but the four-limb lattice stud can improve the energy capacity in a certain extent. The opening rate has little effect on dissipated energy

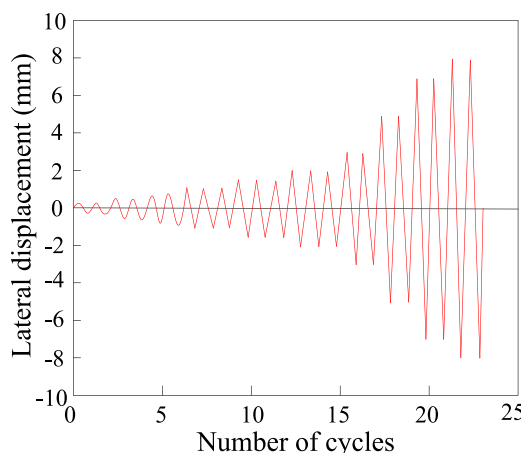
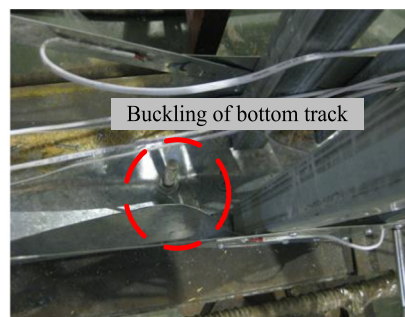


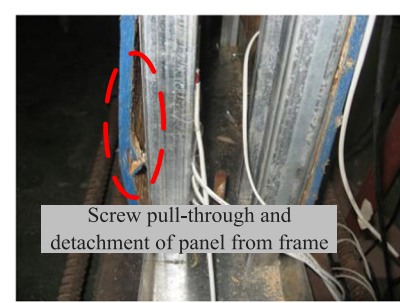
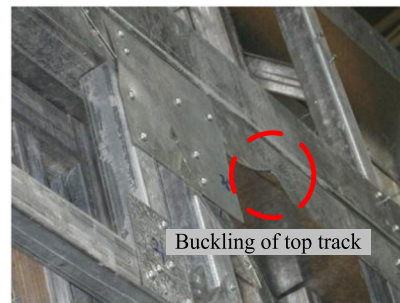
Fig. 5. Loading history.



(a) Specimen CFSTT0

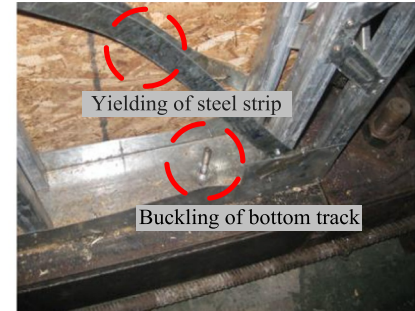
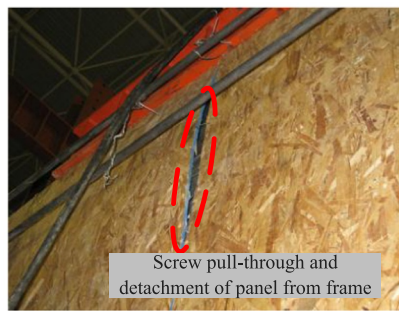
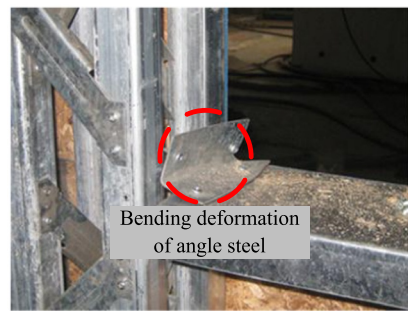


(b) Specimen CFSTT1



(c) Specimen CFSTT2

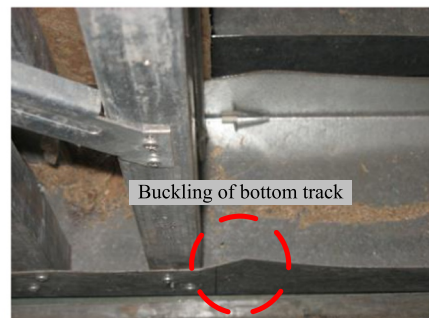
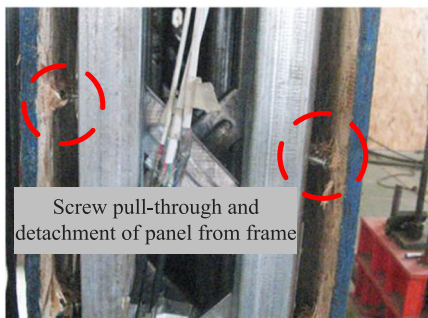
Fig. 6. Failure modes of all specimens.,.



(d) Specimen CFSTT3



(e) Specimen CFSTT4



(f) Specimen CFSTT5

Fig. 6. (continued)

4.1. Material modeling

Although the cold-formed thin-walled steel is considered as an orthotropic material due to the different stress-strain responses corresponding to longitudinal and transverse directions [33], considering only the former in the numerical models is adequate. The maximum longitudinal strains (ϵ_z) reach to the nonlinear curve area, while the maximum transverse strains (ϵ_y) were still in the linear part. The stresses (σ) and strains (ϵ) curves were obtained from the coupon tests as depicted in Fig. 3. The constitutive models of steel were simplified as bi-linear model.

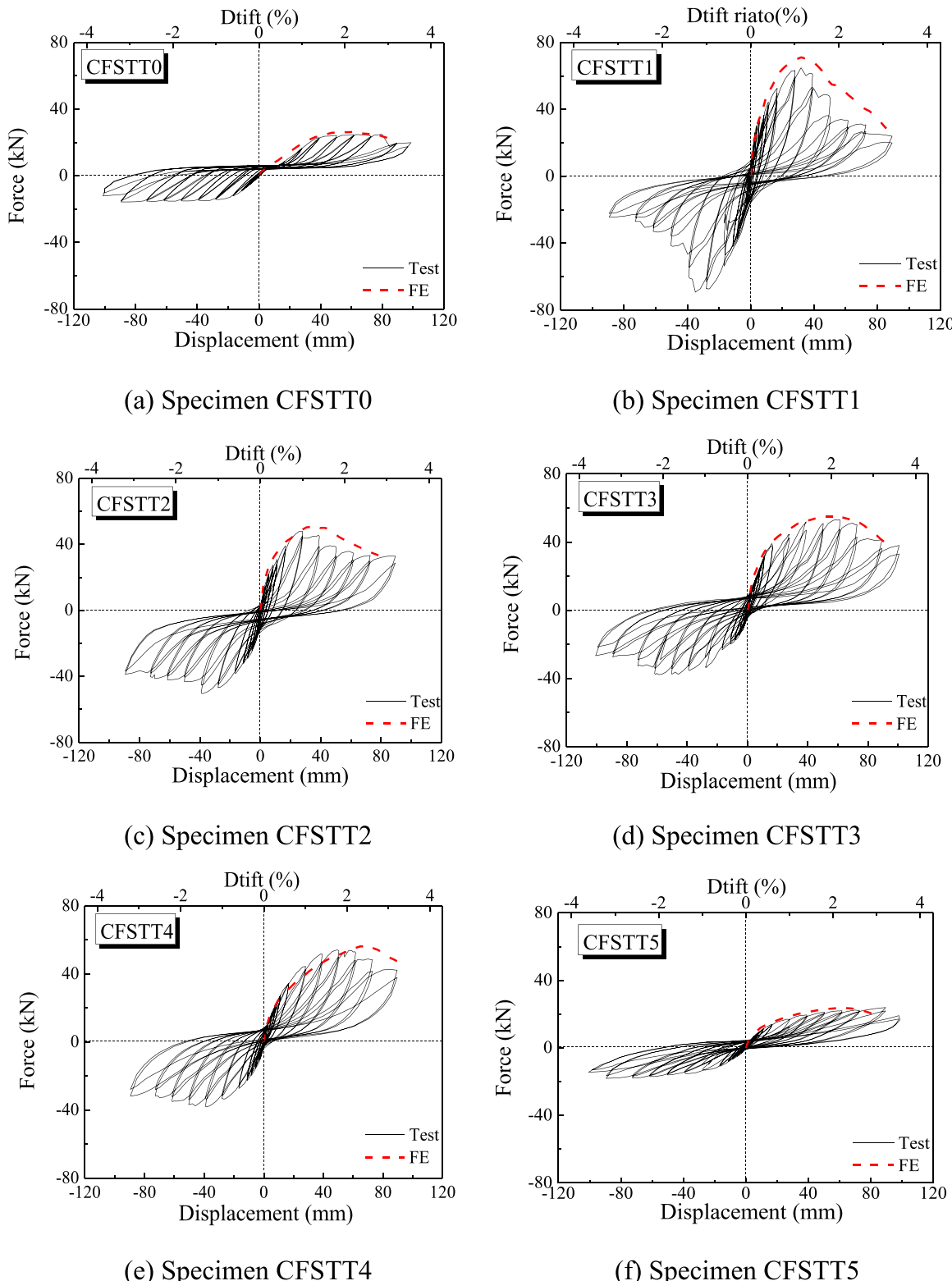
Wood is an anisotropic material, but its mechanical properties will be changed when it is processed into OSB panel. Thus, OSB panel is considered as an isotropic elastic material in FE models in this paper according to the Easley et al. [34].

4.2. Numerical modeling of CFSTT shear wall

Because of the characteristic of the OSB panel, S4R shell elements would be an effective element type to simulate its deformation features. For the steel tube, stripe, track and V-shaped connector, using S4R shell

elements would be proper for analyzing the stress. The S4R element had six degrees of freedom per node and provided an accurate solution to most applications. Mesh convergence studies were also conducted to obtain a reasonable mesh density which provided reliable results with less computational time. The FE mesh for typical components of CFSTT shear walls was shown in Fig. 12. Five regular elements were meshed on V-shaped connector to achieve accurate mechanical behavior. Partition command for geometric elements was used to divide the structural components to achieve mesh convergence. Both material non-linearity and geometric imperfections were taken into considering in the analytical and the Newton-Raphson equilibrium iteration method was adopted in the solution [35].

Considering the failure pattern of the specimens, the screw connection interaction between the steel components and the OSB panels was stimulated using Spring2 element [36]. The Spring2 element used by establishing a spring between two points, and the action direction of spring was fixed towards to a direction which the FE model required. Each screw was stimulated by three spring element including an axial spring and two shear springs. The spring stiffness was tested by the connection test results in Ref. [28]. The screw connection interaction between the steel components was stimulated using “Tie” and the

Fig. 7. Load (P)-displacement (Δ) relationships of test specimens.

surface to surface contact was used to model the contact between framing and sheathing. In the bottom of specimens, three displacements and moments along the axis x , y , z were constrained. The top track was assumed without displacement along the out of plane directions. In the interest of reflecting the actual loading condition, two types of load consisting of axial pressure and lateral displacement were applied in two steps: axial force was imposed on the top track at the first step, and

then a lateral displacement and an axial force were imposed on the shear wall at the second step simultaneously.

4.3. Test verification

Test results obtained from CFSTT shear walls were used to evaluate the effectiveness and accuracy of the numerical modeling. A

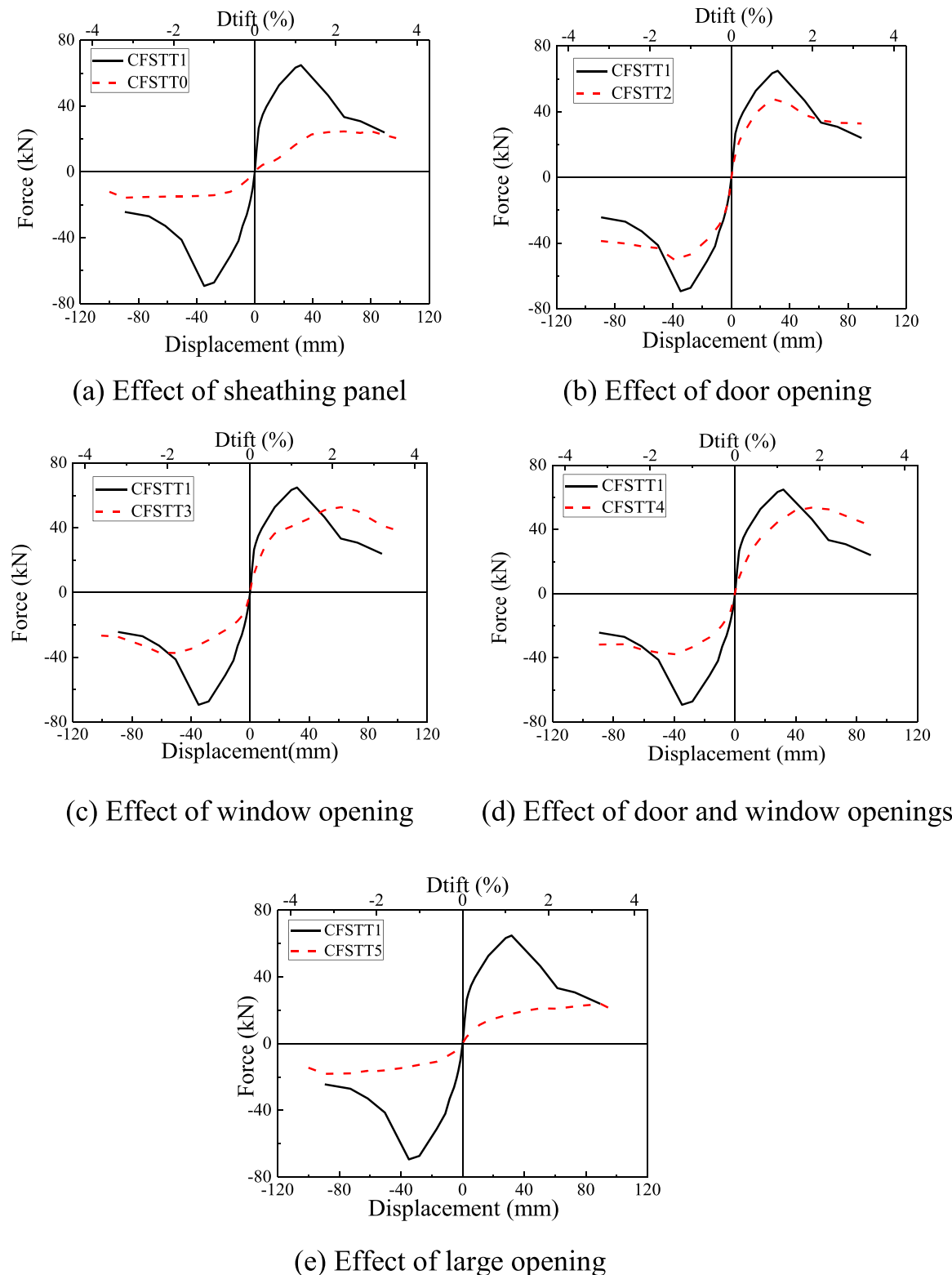


Fig. 8. Load (P)-displacement (Δ) envelope curves of test specimens.

comparison on failure pattern between the experiments and numerical modeling was carried out, as illustrated in Fig. 13. The failure modes of CFSTT shear walls were consistent with the predicted results. It can be seen from Fig. 12 that different types of CFSTT shear walls led to different failure modes. The FE analysis behaved a good consistent with the test results in term of the location of the local buckling. All specimens had achieved an acceptable level of accuracy and the tests were

stopped owing to large deformation and bulking. No unexpected failures exhibited and all the specimens performed satisfactorily.

The availability and accuracy of the FE modeling technique were validated by comparing the numerical analysis results with the test data. Fig. 6 also gave the comparisons between numerical (dashed lines) and experimental (solid lines) load-displacement curves. Comparison of the envelope curves of the hysteresis responses showed that

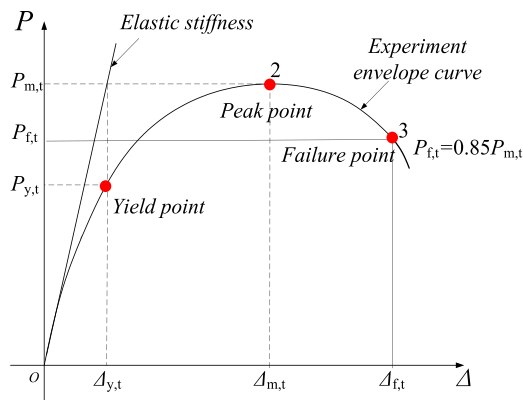


Fig. 9. Characteristic points of specimens.

the numerical results were agreed well with those of tests. The difference between the FE analytical and experimental results was possibly arisen from the difference in the imperfection, site condition and material property between the test specimens and FE models. Generally speaking, the predicted force-displacement curves all specimens were in good agreement with the test curves.

5. Parametric analyses

A numerical analysis was taken by ABAQUS software to discuss the effects of five parameters on the performance of the CFSTT shear walls in this section. The main factors that affect the behavior of this type of structure were determined.

Based on the FE models, a series of parametric investigation of the main variables in a structure design CFSTT shear walls was conducted to determine the discipline on the shear bearing capacity, corresponding displacement, and elastic stiffness. Five parameters could influence the properties of the CFSTT shear walls, consisting of: the stitching method of OSB panel, number of X-shaped bracing, setting of four-limb lattice stud, OSB panel thickness, and wall sheathing type.

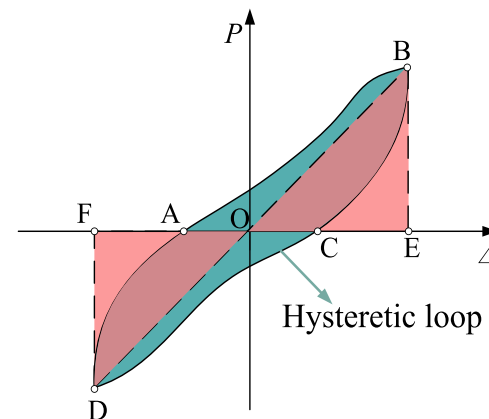
The base model used for comparing the performance of parametric models is CFSTT1.

5.1. Stitching method of OSB panels

The size of the OSB panels produced by the manufacturer is fixed. So the dimensions of OSB panel need to be combined according to the construction requirements in engineering practice. This paper considers a whole panel as contrast indicated that shear bearing capacities and elastic stiffness of two stitching methods of OSB panels had slight

Table 4
Energy dissipation of specimens at limit state.

Specimen	Limit state	Δ/Δ_y	W_{total} (kN-mm)	ξ_e	E_e
CFSTT0	Peak load stage	13	3542	0.061	0.382
	Failure load stage	16	4871	0.064	0.402
CFSTT1	Peak load stage	7	7204	0.209	1.3165
	Failure load stage	9	11,440	0.117	0.734
CFSTT2	Peak load stage	7	6950	0.117	0.735
	Failure load stage	9	9398	0.112	0.706
CFSTT3	Peak load stage	11	11,078	0.106	0.665
	Failure load stage	13	14,680	0.105	0.663
CFSTT4	Peak load stage	11	8070	0.428	2.689
	Failure load stage	16	14,284	0.326	2.049
CFSTT5	Peak load stage	11	9645	0.299	1.876
	Failure load stage	16	11,750	0.203	1.277

Fig. 10. Idealized P - Δ hysteretic relationship.

difference. Thus stitching several OSB panels together is a reliable measure. Two stitching methods of OSB panel including using a whole OSB panel (CFSTT1-W) and stitching several OSB panels together (CFSTT1-S) were investigated to verify the rationality of engineering practice in the process of simulation (seen in Fig. 14). Then the horizontal load-displacement curves are depicted in Fig. 15. The results showed that the shear bearing capacities and elastic stiffness of two stitching methods of OSB panels had slight difference. It can be concluded that the stitching method of the OSB panels had little effect on the elastic stiffness and shear bearing capacity of the shear wall, but it had a certain extent effect on the stress distribution of the panel (seen in Fig. 16). Therefore, the dimensions of OSB panel can be combined according to the construction requirements and convenience in engineering practice.

Table 3
Characteristic values on envelop curves.

Specimen	Yielding point		Peak point		Failure point		μ	Elastic stiffness (N/mm)
	Drift (%)	$P_{y,t}$ (kN)	Drift (%)	$P_{m,t}$ (kN)	Drift (%)	$P_{f,t}$ (kN)		
CFSTT0(+)	0.93	15.11	2.20	24.56	2.99	20.88	3.39	10.65
CFSTT0(-)	0.60	12.11	3.20	18.74	3.44	15.93	5.75	7.35
CFSTT1(+)	0.34	40.12	1.01	74.22	1.32	63.09	4.28	5.97
CFSTT1(-)	0.30	33.04	1.01	74.10	1.46	62.99	4.88	5.62
CFSTT2(+)	0.32	27.48	1.36	54.80	1.59	46.58	5.50	0.95
CFSTT2(-)	0.30	29.16	1.37	50.56	1.99	42.98	6.64	1.06
CFSTT3(+)	0.45	34.01	2.10	53.21	2.72	45.23	6.11	5.05
CFSTT3(-)	0.30	17.62	2.10	37.76	2.70	32.10	9.03	3.93
CFSTT4(+)	0.39	27.25	1.77	54.12	2.75	46.00	6.78	4.94
CFSTT4(-)	0.31	20.16	1.37	38.15	2.56	32.43	8.15	4.10
CFSTT5(+)	0.45	12.08	3.19	23.90	4.12	20.31	5.81	1.67
CFSTT5(-)	0.40	8.11	3.20	18.07	3.47	15.36	8.71	1.32

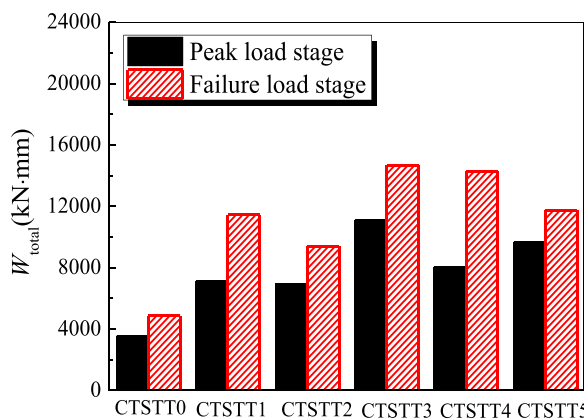


Fig. 11. Total energy dissipation for the test specimens.

5.2. Number of X-shaped bracing

Projects usually employ one X-shaped bracing to improve the bearing capacity of shear wall. While, only one X-shaped bracing won't make for a good construction when the wall is too long. So some designers suggested using two or three X-shaped bracing to avoid the problem. The influence of number of X-shaped bracing on the shear bearing capacity and elastic stiffness of the CFSTT shear wall is shown in Fig. 17. The numerical models with various number of X-shaped bracing ($n = 0, 1, 2$ and 3) were conducted. Then Fig. 18(a) depicted the horizontal load-displacement curves. According to the numerical results, when one X-shaped bracing was set on both sides of the shear wall, its shear bearing capacity and elastic stiffness respectively increased by 70.2% and 91.6%, compared to the shear wall without X-shaped bracing. However, when the CFSTT shear wall adopted more than one X-shaped bracing, the shear bearing capacity and elastic stiffness of the shear wall were not affected notably. It indicated that one X-shaped bracing was enough to improve the shear bearing capacity and elastic stiffness, in case that there would be no four-limb lattice studs setting to strengthen the interior wall studs which were connected to the end of the steel strip. In order to avoid the aforementioned

circumstance and to take full use of the increasing X-shaped bracing, strengthening the end of the steel strip by four-limb lattice studs was preliminarily recommended by designers (seen in Fig. 17 (e,f)). Hence, Fig. 18(b) illustrates the analytical results of their corresponding strengthened models to present a considerable reference for the engineering practice. The results demonstrated that the shear bearing capacities of Model-X2-strengthen and Model-X3-strengthen increased respectively by 36.8% and 49% with respect to Model-X1, while improvements of 29% and 45% in elastic stiffness were observed as well. Accordingly, it can be figured out that strengthening the wall stud in the end of steel strip is an effective method to increase the contribution of X-shaped bracing.

5.3. Four-limb lattice stud

The four-limb lattice stud is a significant design parameter in practical engineering. In this paper, in order to achieve the goal of the variation of four-limb lattice studs in the FE models, four-limb lattice studs of specimens CFSTT2, CFSTT3, CFSTT4 and CFSTT5 (except for four-limb lattice studs on the both side of the specimens) were replaced by double-limb lattice studs. The models without four-limb lattice studs on the side of opening were defined as CFSTT0. Fig. 19 provided a comparison of the horizontal load versus later displacement ($P-\Delta$) relationship with the change of four-limb lattice studs. The analysis results indicated that the shear bearing capacities of model CFSTT2, CFSTT3, CFSTT4 and CFSTT5 with double-limb lattice studs decreased by 3.6%, 4.7%, 26.5% and 16.1% with respect to specimens with four-limb lattice studs. The reason for these simulation results were that the shear bearing capacity of the CFSTT shear wall would be enhanced by setting four-limb lattice studs.

5.4. Thickness of OSB panel

Different thickness of OSB panel including 6, 8, 15 and 20 mm were investigated in this section. In this part, the strength of sheathing-to-frame connections had been improved to meet different OSB panel thickness. Fig. 20 showed that when the OSB panel thickness of shear walls changed from 6 mm to 8, 15, 20 mm, the elastic stiffness of the shear walls was raised by 30%, 47%, 89%, respectively, and the

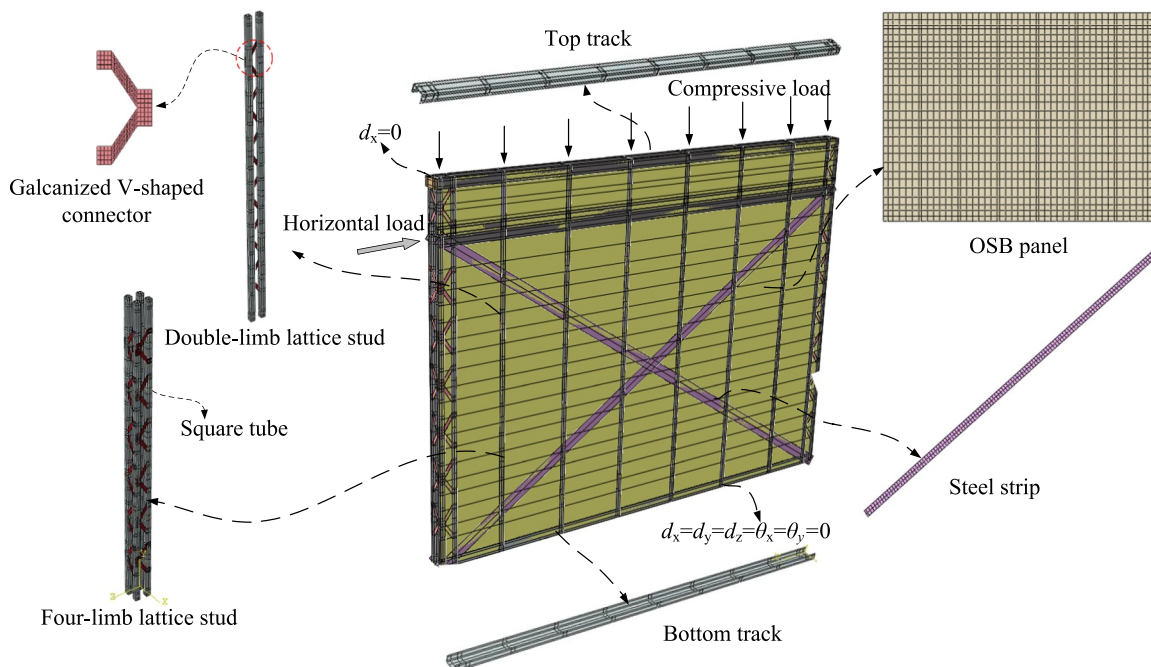


Fig. 12. FE analysis model.

improvements in shear bearing capacity were respectively 18.4%, 30.8%, 41.3%. This result demonstrated that the thickness of OSB panel had a significant influence on the shear bearing capacity and elastic stiffness.

5.5. Type of wall sheathing

At the same size of shear walls, five models with different types of sheathing including OSB panel, thin steel sheathing (TS), gypsum board (GB), plywood panel (PLY) and bamboo plywood panel (BPLY) were considered. Similarly, the strength of sheathing-to-frame connections had been changed to match different sheathing types. Table 5 listed the material characteristics of various panels. The horizontal load versus

displacement curves for the different types of panel are shown in Fig. 21. The results indicated that the model adopting OSB panels had lower shear bearing capacity than that of models adopting PLY panels and BPLY panels, but the model adopting OSB panels had higher elastic stiffness. It can be found that the TS panel and GB panel had highest and lowest shear bearing capacity and elastic stiffness, respectively. That is to say, when the TS panels are used in the shear wall, it has good shear bearing capacities and elastic stiffness, while the model adopting PB panels has poor performance when compared with other panels. Therefore, the above mentioned results showed that the ductile material can be used as sheathing of CFSTT shear wall in engineering practice, and the PB panel should be used carefully as the wall sheathing.

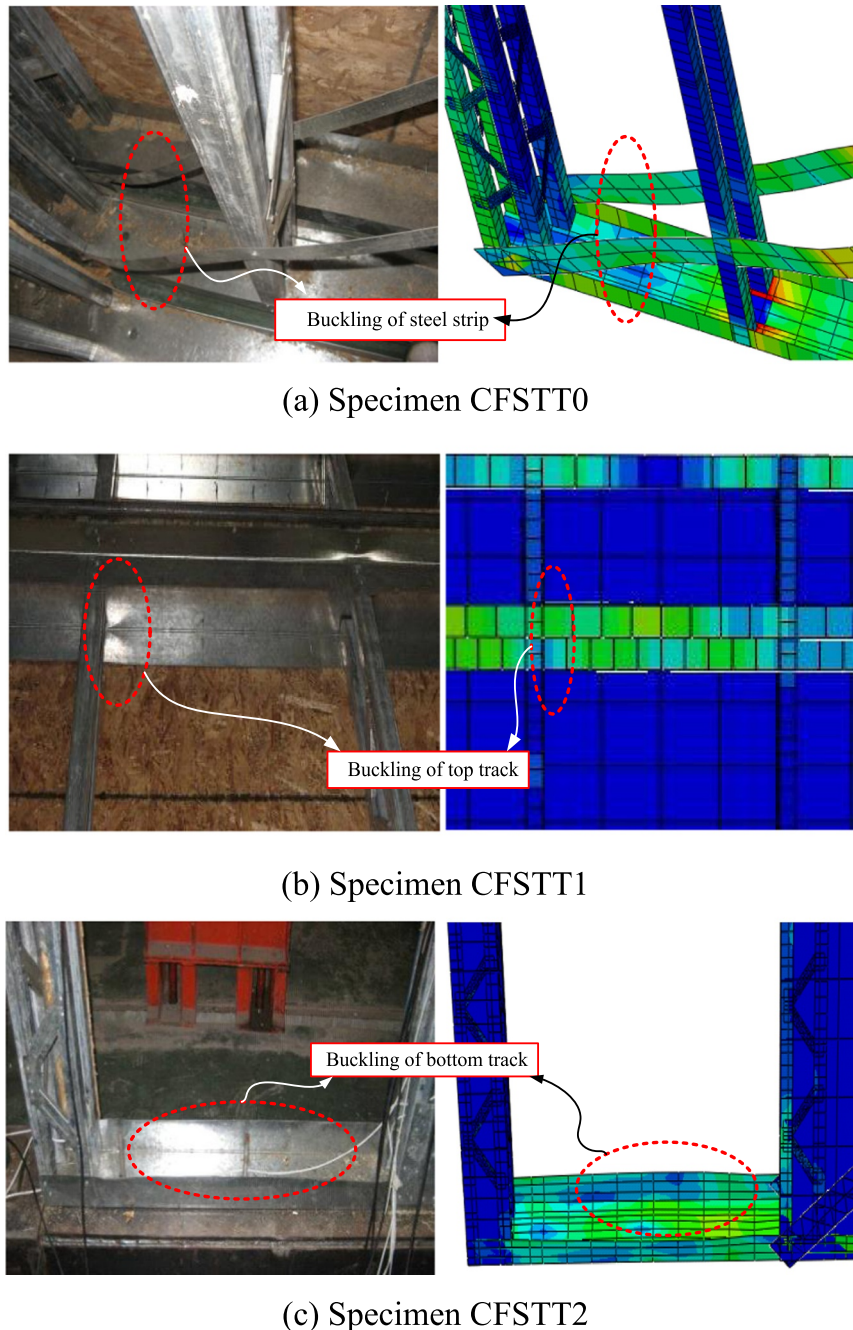
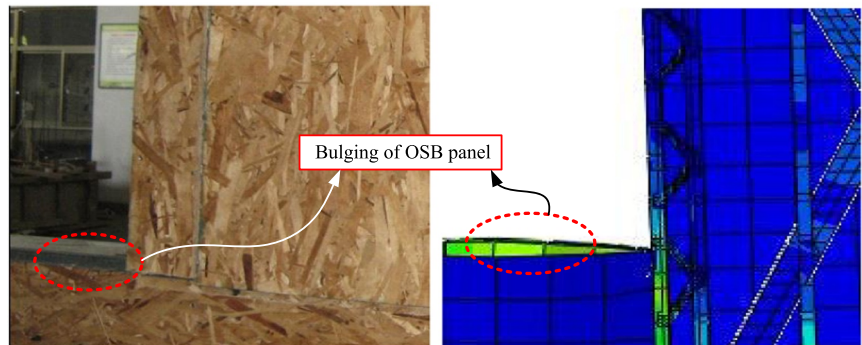


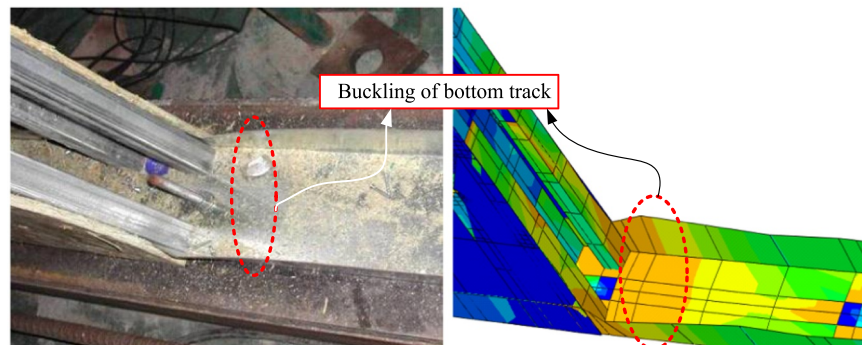
Fig. 13. Observed and predicted failure modes.



(d) Specimen CFSTT3



(e) Specimen CFSTT4



(f) Specimen CFSTT5

Fig. 13. (continued)

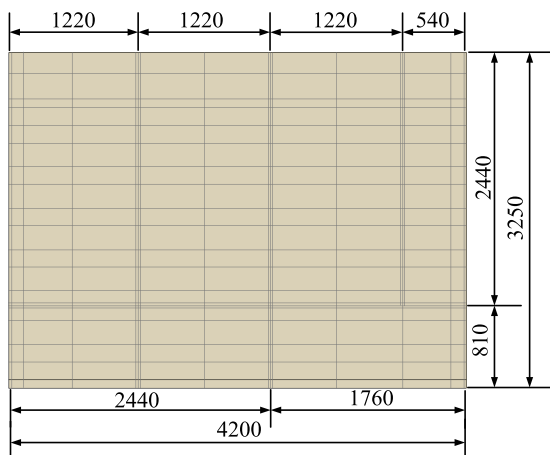
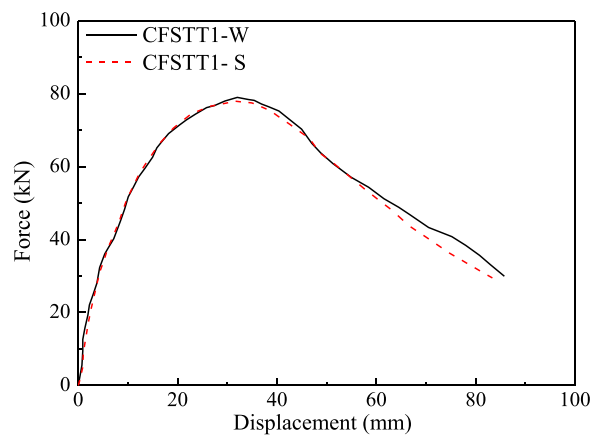


Fig. 14. Assembly of OSB panels.

Fig. 15. Effect of stitching methods of OSB panels on $P-\Delta$ relations for CFSTT shear walls.

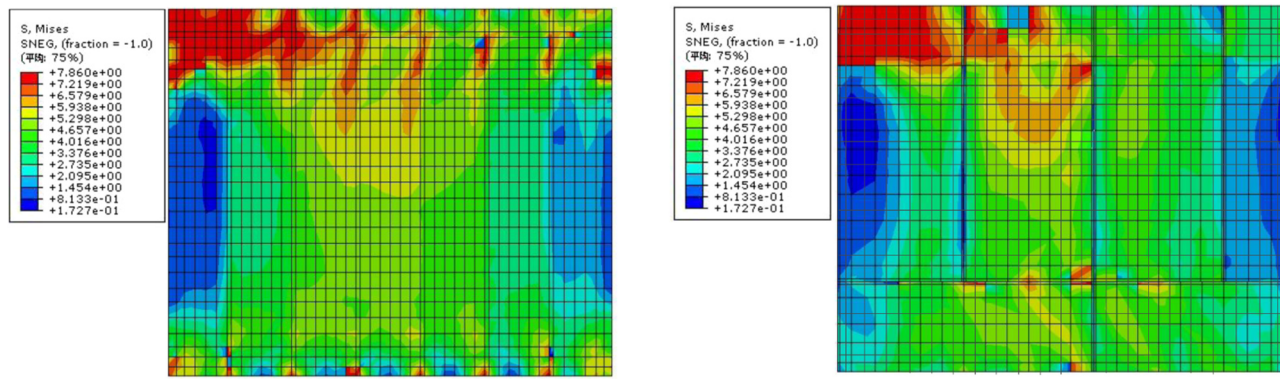


Fig. 16. Stress distribution for different OSB panel combination methods.

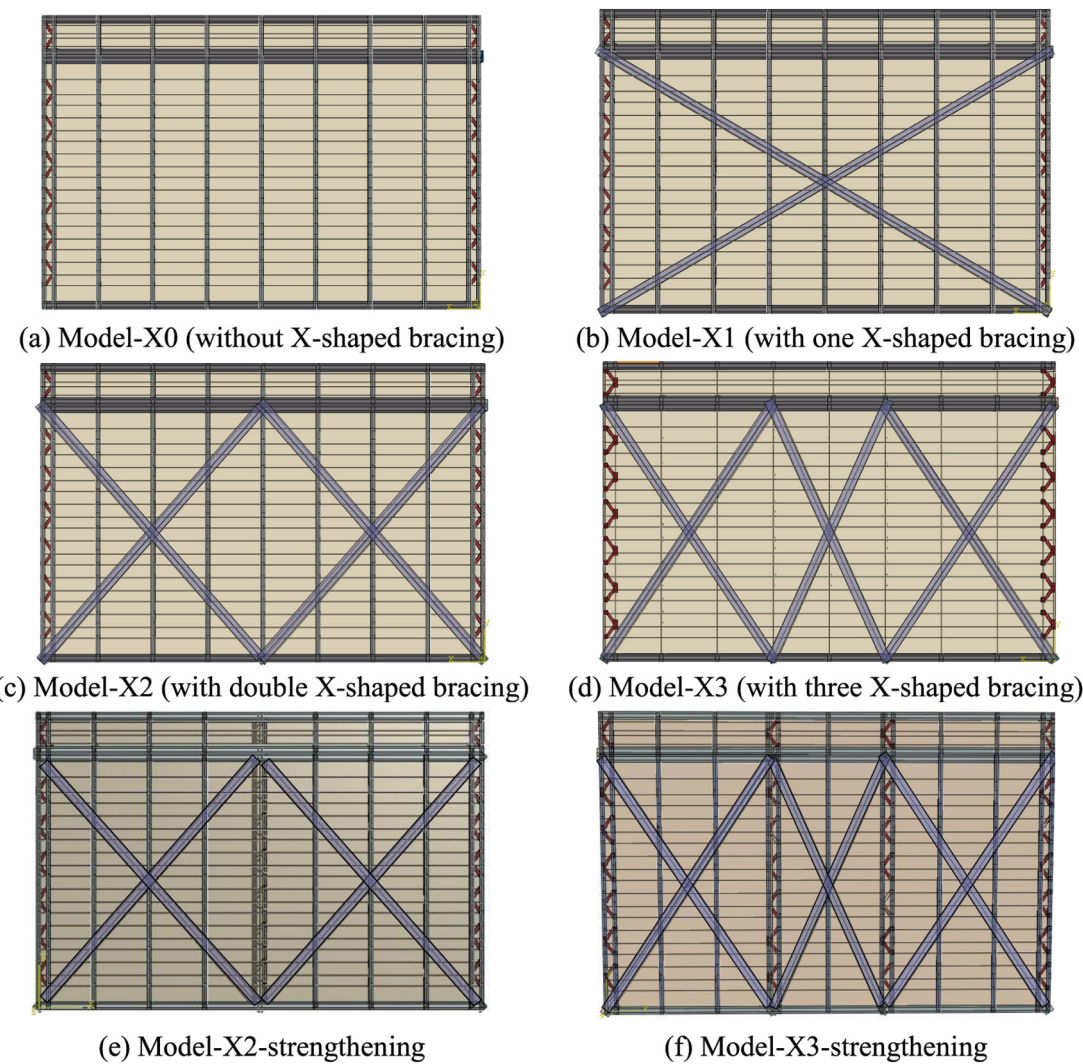
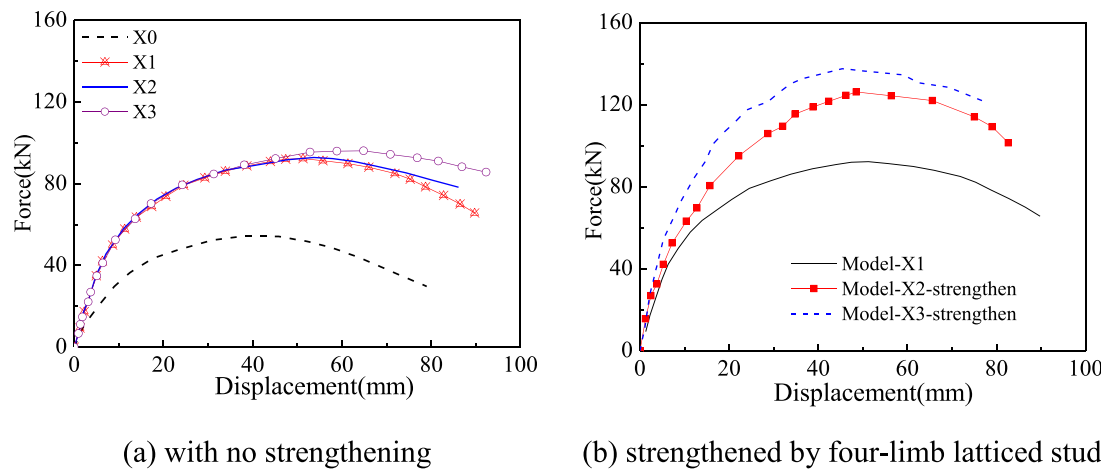
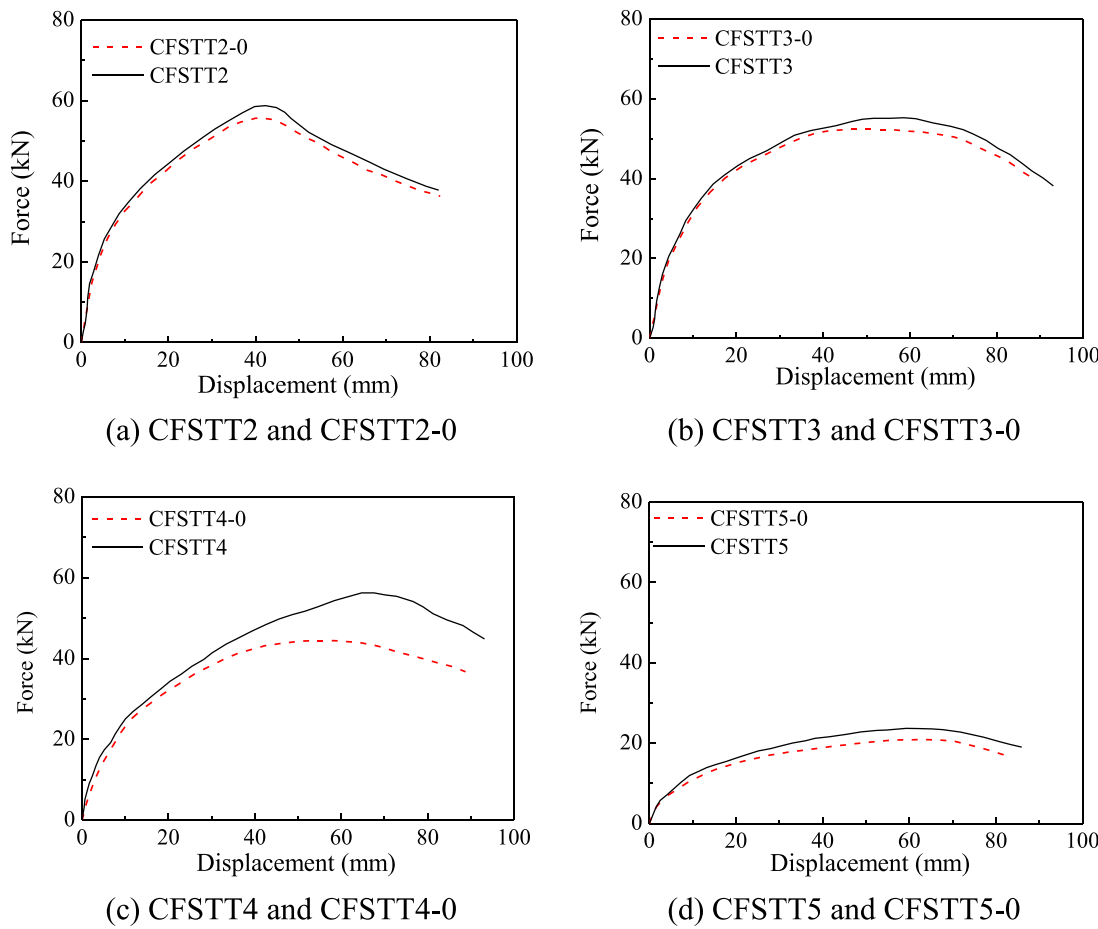


Fig. 17. Number of X-shaped bracing.

Fig. 18. Effect of X-shaped bracing number on $P\Delta$ relations for CFSTT shear walls.Fig. 19. Effect of four-limb lattice stud on $P\Delta$ relations for CFSTT shear walls.

6. Discussion

6.1. Opening

According to the above studies, the tension field force was larger around the opening corner; while the stress in other places was not obvious. Therefore, the cracks and local buckling of the OSB panels were discovered within the vicinity of opening. Besides, the buckling of specimens CFSTT2–CFSTT5 appeared first at lower load levels owing to large stress resulted from wall opening. In order to offset the above deficiencies, it can be considered to replace the sharp corner with

circular arc in the practical design. It may be a reliable method to reduce the stress around the opening corner. Moreover, this method may be possible to postpone the failure proceeding of the OSB panels and thus improve the ductility and shear bearing capacity of the CFSTT shear wall.

6.2. Strengthening of X-shaped bracing

Fig. 18 investigated the influence of X-shaped bracing on the $P\Delta$ relationship of CFSTT shear wall. Strengthening the shear wall by X-shaped bracing may be an effective approach to heighten its

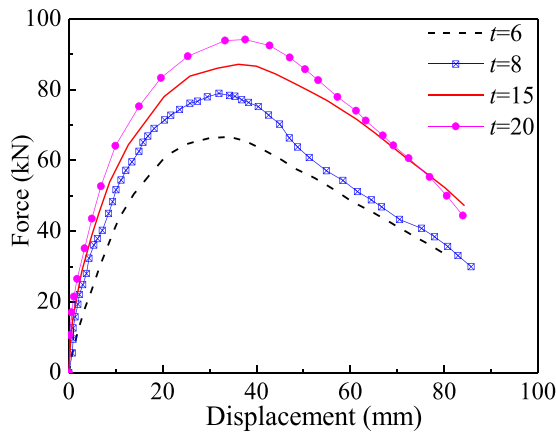


Fig. 20. Effect of thickness of OSB panel on $P\Delta$ relations for CFSTT shear walls.

Table 5
Material properties of different wall panels in parametric analyses.

Panel type	Elastic modulus E (N/mm ²)	Yield strength (N/mm ²)	Poisson ratio ν
OSB	3500	7.86	0.30
TS	206,000	320	0.30
GB	1125	0.66	0.23
PLY	4000	25	0.15
BPLY	7110	55	0.13

Note: TS-thin steel sheathing; GB-gypsum board; PLY-plywood panel; BPLY-bamboo plywood panel.

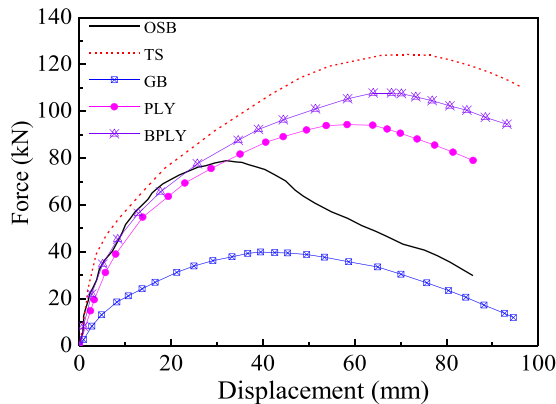


Fig. 21. Effect of sheathing type on $P\Delta$ relations for CFSTT shear walls.

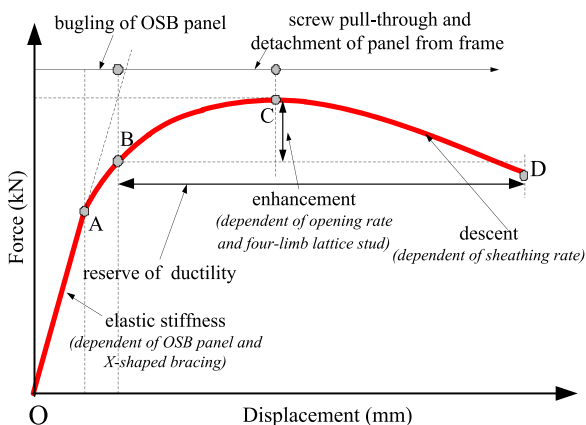


Fig. 22. Typical $P\Delta$ curve of CFSTT shear wall.

performance. Moghimi and Ronagh [37,38] had put forward an effective method to enhance CFS skeleton and indicated that strap bracing could be adopted to provide a considerable amount of shear bearing capacity after the appearance of the signs of buckling. Moreover, based on the above parametric analysis, in case of no four-limb lattice studs were set to strengthen the interior wall studs which were connected to the end of the steel strip, setting up one X-shaped bracing was the most economical measure. Besides, the fracture of the steel strip mostly occurred at the joint with wall studs, which were connected by self-drilling screws. This phenomenon was attributed to the stress concentration around the self-drilling screws. Therefore, widening the cross section of steel strip and designing the connection part into dumbbell-shape to decrease its stress was suggested in this paper to enhance the strength of X-shaped bracing.

6.3. Strengthening of four-limb lattice stud

According to the analysis of Section 5.3, four-limb lattice studs for the CFSTT shear wall may be another reliable method to enhance its shear resistance. Despite the fact that specimens CFSTT2 and CFSTT3 had similar opening rate where $\alpha = 13.8\%$, and 13.9% , respectively, the experimental result (as depicted in Table 4) showed that the total dissipated energy W_{total} of specimen CFSTT3 was increased by 51.5%, compared to specimen CFSTT2. Moreover, although the specimen CFSTT5 has a large opening, its energy dissipation capacity is not significantly lower than that of specimen CFSTT1. These might because that setting up four-limb lattice stud can improve the energy dissipation and structural integrity of the CFSTT shear wall. According to the FE analysis results in Fig. 19, the shear bearing capacity and its corresponding displacement of the analysis model with four-limb lattice studs are relatively larger than those of model without four-limb lattice studs.

Furthermore, when the steel strips fractured, the wall studs showed no apparent buckling, which demonstrated that there was too much redundancy in strength for the wall studs. It can be conceived that the difference in strength level between the thin steel strips and the wall studs seem a little large, which would stifle the strength of wall studs. Therefore, designing proper steel strips to match with the strength of the wall studs is of great importance and it still needs to be further investigated.

6.4. Strengthening of infill material

In practical engineering, complicated detail of shear walls is required to meet the requirements of thermal and sound insulation. However, the CFSTT shear wall proposed in this paper held hollow section and could not meet the above mentioned demands. Hence, some scholars were focused on the studies of the wall filled with various light materials, which is recommended in this section either. In some wall productions, expanded polystyrene (EPS) materials, extruded polystyrene (XPS) stuffs, and insulation cotton was attempted to place inside the cavities or to cover on the outside surfaces of the steel frames. Besides, a method that using sprayed light weight mortar EPS boards was introduced according to Ref. [8]. Based on the above literatures, it can be found that using reasonable filling materials could also strengthen the stability of the CFSTT shear wall, and thereby its load carrying capacity as well. This method can not only reduce the carbon footprint but also can improve living standards significantly.

6.5. Analysis of $P\Delta$ curves

A standard $P\Delta$ curve of CFSTT shear wall under axial and lateral loads was observed based on amounts of test results and numerical analysis (seen in Fig. 22). Test and FE results indicated that the shape

and trend of the $P\Delta$ curves are related to the various parameters and each curve could be divided into four parts:

- (1) The elastic stage (OA). The bearing capacity has an approximate linear relationship before the lateral displacement reaches the point A. The slope of the OA is the elastic stiffness K_i of the specimen. The elastic stiffness may be improved by X-shaped bracing and OSB panel; while the elastic stiffness may be reduced with the increasing of opening rate.
- (2) The elastic-plastic stage (AB). The force undertaken by shear wall shows a nonlinear relationship with the displacement. This phenomenon indicates that the CFSTT skeleton steps into elastic-plastic stage. Finally, the CFSTT shear wall goes to the yielding strength with the $P\Delta$ curve reaching point B.
- (3) The strain-hardening stage (BC). With the load and displacement increasing, the shear bearing capacity of the CFSTT shear wall is dramatically improved. In this stage, local buckling of the OSB panels, X-shaped, bottom and top tracks are observed. Besides, some screws have been pulled out. The vertical distance of points B and C is related with X-shaped bracing, opening rate, four-limb lattice stud and OSB panel.
- (4) The descent stage (CD). Owing to the cracks of OSB panel and pull-out of screws, the $P\Delta$ curve of the CFSTT shear wall under axial and later load exhibits a feature of descent beyond the peak load. Experimental and numerical data indicates that the slope of the descent is correlated to the sheathing rate. The higher sheathing rate, the larger level of descent is.

For the curve of the CFSTT shear wall, the reserve of ductility (defined as the horizontal distance of points B and D) is related with the opening rate, X-shaped bracing and four-limb lattice stud. After reaching the shear bearing capacity, the load of the shear wall decreases slowly which shows a feature of gentle descent. This phenomenon is attributed to the excellent ductility property of thin-walled steel studs.

7. Conclusions

This paper studied the seismic performance of CFSTT shear walls. A nonlinear FE modeling was developed and verified by test data, and then an extensive parametric analysis on the CFSTT shear wall was conducted. According to the experimental and analytical results in this paper, the following conclusions can be drawn:

- (1) Local buckling of the top and bottom tracks, tearing and detaching of OSB panels, as well as fracture of X-shaped bracing were the predominant failure modes of CFSTT shear wall. For CFSTT shear walls with openings, which were more typicality of real conditions, the failure modes of OSB panels were characterized by cracking around the openings.
- (2) The ultimate strength and elastic stiffness of the CFSTT shear walls with double-side OSB panels were significantly improved when compared with pure CFSTT skeleton wall indicating that the diaphragm effect had a favorable influence on hysteretic behavior and energy dissipation capacity of the CFSTT shear walls. Nevertheless, the wall openings would weaken seismic behavior and energy-dissipating capacity of the CFSTT shear walls.
- (3) The FE modeling on CFSTT shear wall was established and verified by the experimental data in term of failure pattern and load-displacement relation curves in this study. Thus, it proved that the FE models could be used to predict the seismic response of the type of shear wall with an acceptance precision.

- (4) The extensive numerical parameter analysis results showed that the shear bearing capacity and elastic stiffness of the CFSTT shear wall were obviously affected by number of X-shaped bracing, four-limb lattice stud, thickness of OSB panel and the type of sheathing. Different stitching methods of OSB panel had slight effect on the shear bearing capacity and elastic stiffness of the CFSTT shear wall.

Acknowledgments

This work described in paper is supported by the National Natural Science Foundation of China (Project 51478158) and the New Century Excellent Talents in University (Project NCET-12-0838); the authors greatly appreciated the support.

References

- [1] C. Yu, G.W. Yu, Experimental investigation of cold-formed steel framed shear wall using corrugated steel sheathing with circular holes, *J. Struct. Eng.* 142 (12) (2016) 04016126.
- [2] CAN/CSA S136-01 (R2007) North American specification for the design of cold formed steel structural members. Canadian Standards Association.
- [3] L. Fiorino, S. Shakeel, V. Macillo, R. Landolfo, Behaviour factor (ϕ) evaluation the CFS braced structures according to FEMA P695, *J. Constr. Steel Res.* 138 (2017) 324–339.
- [4] Y.K. Lee, T.H. Miller, Axial strength determination for gypsum-sheathed, cold-formed steel wall stud composite panels, *J. Struct. Eng.* 127 (6) (2001) 608–615.
- [5] Y.S. Tian, J. Wang, T.J. Liu, Axial load capacity of cold-formed steel wall stud with sheathing, *Thin-Walled Struct.* 45 (5) (2007) 537–551.
- [6] Y.S. Tian, J. Wang, T.J. Lu, C.Y. Barlow, An experimental study on the axial behavior of cold-formed steel wall studs and panels, *Thin-Walled Struct.* 42 (2004) 557–573.
- [7] X.X. Wang, J.H. Ye, Cyclic testing of two- and three-story CFS shear-walls with reinforced end studs, *J. Constr. Steel Res.* 121 (2016) 13–28.
- [8] M. Nithyadharan, V. Kalyanaraman, Behavior of cold-formed steel shear wall panels under monotonic and reversed cyclic loading, *Thin-Walled Struct.* 60 (11) (2012) 12–23.
- [9] V. Macillo, L. Fiorino, R. Landolfo, Seismic response of CFS shear walls sheathed with nailed gypsum panels: experimental tests, *Thin-Walled Struct.* 120 (2017) 161–171.
- [10] B.W. Schafer, D. Ayhan, J. Leng, P. Liu, D. Padilla-Llano, K.D. Peterman, M. Stehman, S.G. Buonopane, M. Eatherton, R. Madsen, B. Manley, C.D. Moen, N. Nakata, C. Rogers, C. Yu, Seismic response and engineering of cold-formed steel framed buildings, *Structures* 8 (2016) 197–212.
- [11] T. Kim, J. Wilcoski, D.A. Foutch, M.S. Lee, Shaketable tests of a cold-formed steel shear panel, *Eng. Struct.* 28 (10) (2006) 1462–1470.
- [12] Y. Telue, M. Mahendran, Behaviour of cold-formed steel wall frames lined with plasterboard, *J. Constr. Steel Res.* 57 (4) (2001) 435–452.
- [13] S. Reynaud, E. Jose, J. Melissa, N. Hoang, Static racking behavior of plywood, OSB, gypsum, and fiberboard walls with metal framing, *J. Struct. Eng.* 123 (8) (1997) 1079–1086.
- [14] B. Liu, J.P. Hao, W.H. Zhong, H. Wang, Performance of cold-formed-steel-framed shear walls sprayed with lightweight mortar under reversed cyclic loading, *Thin-Walled Struct.* 98 (2016) 312–331.
- [15] Y.Q. Li, J.K. Yang, Study on shear capacity of cold-formed thin-walled steel composite walls with openings, *Adv. Mater. Res.* 374–377 (2012) 1738–1741.
- [16] M. Casafont, A. Arnedo, F. Roure, A. Rodríguez-Ferran, Experimental testing of joints for seismic design of lightweight structures. Part 2: bolted joints in straps, *Thin-Walled Struct.* 44 (2006) 677–691.
- [17] J. Ye, X. Wang, M. Zhao, Experimental study on shear behavior of screw connections in CFS sheathing, *J. Constr. Steel Res.* 121 (2016) 1–12.
- [18] S. Swensen, G.G. Deierlein, E. Miranda, Behavior of screw and adhesive connections to gypsum wallboard in wood and cold-formed steel-framed wallets, *J. Struct. Eng.* 162 (4) (2016) E4015002.
- [19] L. Fiorino, T. Pali, B. Bucciero, V. Macillo, M. Teresa, Terracciano, R. Landolfo, Experimental study on screwed connections for sheathed CFS structures with gypsum or cement based panels, *Thin-Walled Struct.* 116 (2017) 234–249.
- [20] J. Ye, X. Wang, M. Zhao, Experimental study on shear behavior of screw connections in CFS sheathing, *J. Constr. Steel Res.* 121 (2016) 1–12.
- [21] L. Fiorino, M.T. Terracciano, R. Landolfo, Experimental investigation of seismic behaviour of low dissipative CFS strap-braced stud walls, *J. Constr. Steel Res.*, Elsevier Sci. 127 (2016) 92–107.
- [22] O. Iuorio, V. Macillo, M.T. Terracciano, T. Pali, L. Fiorino, R. Landolfo, Seismic response of Cfs strap-braced stud walls: experimental investigation, *Thin-Walled Struct.* 85 (2014) 466–480.

- [23] V. Macillo, O. Iuorio, M.T. Terracciano, L. Fiorino, R. Landolfo, Seismic response of CFS strap-braced stud walls: theoretical study, *Thin-Walled Struct.* 85 (2014) 301–312.
- [24] S.E. Niari, B. Rafezy, K. Abedi, Seismic behavior of steel sheathed cold-formed steel shear wall: experimental investigation and numerical modeling, *Thin-Walled Struct.* 96 (2015) 337–347.
- [25] L. Fiorino, S. Shakeel, V. Macillo, R. Landolfo, Seismic response of CFS shear walls sheathed with nailed gypsum panels: numerical modeling, *Thin-Walled Struct.* 122 (2018) 359–370.
- [26] DB34/T 647-2006, Technical specification for web steel building, Anhui engineering construction standard design office, Hefei, 2007 (in Chinese).
- [27] GB15856-2002, Drilling screws with tapping screw thread, China Plan Press, Beijing, 2002 (in Chinese).
- [28] GB50018-2016, Technical code of cold-formed thin-wall steel structures, China Plan Press, Beijing, 2016 (in Chinese).
- [29] Y. Shi, S.W. Wang, Y.J. Liu, Research on shear behavior of single tapping screw connection in cold-formed thin-wall steel structures, *J. Archit. Civil. Eng.* 31 (2) (2014) 57–64 (in Chinese).
- [30] GB/T228-2010, Metallurg Materials-Tensile testing at Ambient Temperature, Architecture Industrial Press of China, Beijing, 2010 (in Chinese).
- [31] ATC-24, Guidelines for cyclic seismic testing of components of steel structures, Applied Technology Council, Redwood City (CA), 1992.
- [32] JGJ/T 101-2015, Specification for Seismic Test of Buildings, Architecture Industrial Press of China, Beijing, 2015 (in Chinese).
- [33] GB50011-2010, Code for Seismic Design of Buildings, Architecture Industrial Press of China, Beijing, 2010 (in Chinese).
- [34] J.T. Easley, M. Foomani, R.H. Dodds, Formulas for wood shear walls, *J. Struct. Div.* 108 (11) (1982) 2460–2478.
- [35] ABAQUS, Standard user's manual version 6.10, Hibbit, Karlsson & Sorensen, Inc., Pawtucket, RI, 2010, pp. 57–63.
- [36] M. Mahdavianm, W. Zhang, C. Ding, Cyclic simulation of cold-formed steel shear walls with corrugated steel sheathing, Proceeding of the Annual Stability Conference, Orlando, Florida, 2016.
- [37] H. Moghimi, H.R. Ronagh, Performance of light-gauge cold-formed steel strap-braced stud walls subjected to cyclic loading, *Eng. Struct.* 31 (1) (2009) 69–83.
- [38] H. Moghimi, H.R. Ronagh, Better connection details for strap-braced CFS stud walls in seismic regions, *Thin-Walled Struct.* 47 (2009) 122–135.